Effect of Annealing on Upconversion Luminescence of ZnO:Er^{3+} Nanocrystals and High Thermal Sensitivity

Xin Wang,[†,‡] Xianggui Kong,[*,†] Yi Yu,[†] Yajuan Sun,[†] and Hong Zhang[*,§]

Key Laboratory of the Excited State Processes, Changchun Institute of Optics, Fine Mechanics and Physics, Chinese Academy of Sciences, Changchun, 130033, People's Republic of China, Department of Chemistry, Tsinghua University, Beijing, 100084, People's Republic of China, and Van't Hoff Institute for Molecular Sciences, Universiteit van Amsterdam, Nieuwe Achtergracht 166, 1018 WV Amsterdam, The Netherlands

Received: December 18, 2006; In Final Form: July 30, 2007

The effect of annealing on the upconversion luminescence of ZnO:Er^{3+} nanocrystals was investigated in detail. The green and the red upconverted emissions under infrared 978-nm light excitation were remarkably enhanced with an increase of annealing temperature. Moreover, for the sample annealed at 500 °C, the ratio of the intensity of $^2H_{11/2} \rightarrow {}^4I_{15/2}$ emission to that of $^4S_{3/2} \rightarrow {}^4I_{15/2}$ emission increased from less than to more than unity with an increase of the excitation density. However, the same case did not occur to the sample annealed at 700 °C, where the ratio was independent of excitation density except when the excitation density was higher than 42 700 W/cm^2. This distinction was attributed mainly to the difference in energy gap between the $^2H_{11/2}$ and $^4S_{3/2}$ states in the two samples, originating from the local microstructure variation around Er^{3+} ions. In addition, a high thermal sensitivity of 0.0062/°C was obtained in the ZnO:Er^{3+} nanocrystals based on the temperature-dependent fluorescence intensity ratio (FIR) of the green upconverted emission, which would make this material a promising candidate for the nanoscaled thermal sensor of high accuracy and resolution.

Introduction

In recent years, the conversion of infrared (IR) radiation into visible light in rare-earth (RE) ion implanted solid-state nanocrystals has been a focus of intensive research.[1−4] Their potential application covers broad areas, including color displays, short-wavelength lasers, IR quantum counter detectors, optical data reading/storage, optical communications, two-photon fluorescence imaging, and most recently, biomedical diagnostics.[5] In particular, the development of novel fluorescent RE-doped nanocrystals has been promoted strongly because of their application in fluorescent labels based on their superior optical properties, such as sharp emission lines, no photobleaching, low background, and long lifetimes suitable for time-resolved techniques, in contrast with conventional organic fluorophores.[6] Relevant research on RE-doped nanocrystals and their upconversion luminescence properties have thus been boosted.[7−11]

Zinc oxide is not only a wide-direct-gap semiconductor material but also a promising host candidate for RE ions and transition-metal ions, which has potential application in optoelectronic devices, waveguides, optical amplifiers, biomarkers, and magnetic memory devices.[12−19] However, despite the extensive studies on Er-doped ZnO nanostructure materials or thin films for optical amplifiers at 1.54 μm in the waveguide structure were reported by Spanhel[12−13] and Komuro,[14,15] few reports on the downconverted or upconverted visible luminescence from Er-doped ZnO have appeared in the literature.[14,20] The low phonon-energy and appropriate coordination of oxygen around Er makes ZnO suitable for the realization of efficient upconversion luminescence. Furthermore, trivaluable erbium ions are excellent dopant and have the capability of converting IR radiation to visible light efficiently because of favorable electronic energy levels (such as $^4I_{9/2}$ and $^4I_{11/2}$) that are easily accessible with near-IR radiation from low-cost commercially available diodes.

Alternatively, fluorescent temperature sensing techniques have been studied widely for their application in electrical power station, oil refineries, coal mines, and building fire detection.[21−23] A fluorescent sensor that makes use of temperature-dependent fluorescence properties from luminescence material can overcome the interference of strong electromagnetic noise, hazardous sparks, and corrosive environment that are inaccessible to traditional temperature-measurement methods such as thermocouple detectors. Fluorescent temperature sensing techniques include the temperature-dependent fluorescence lifetime and FIR, which involve suitable optical materials including phosphors, crystals material, and RE-doped optical fibers. Especially, the FIR technique, independent of signal losses and fluctuation in the excitation intensity, has the potential to improve the measurement accuracy and resolution significantly.[23] This technique may be applied to a system where two closely spaced energy levels are involved following a Boltzmann-type population distribution.[23] Because the emission intensities are proportional to the population of two thermally equilibrious levels, FIR is expressed by $FIR = B \exp(-\Delta E/k \cdot T)$, where B is a constant, ΔE is the energy difference between the two levels, k is the Boltzmann constant, and T is the absolute temperature.[23,24] Because of the special 4f energy levels of trivaluable erbium ions, the Er-doped matrix is favorable as the thermal sensing fluorescent material. Nanosized materials doped with Er ions are thus promising candidates for the thermometry or nanoscaled

* To whom correspondence should be addressed. Tel: +86-431-8617 6313. Fax: +86-431-8462 7031. E-mail: xgkong14@ciomp.ac.cn; h.zhang@uva.nl.

† Changchun Institute of Optics, Fine Mechanics and Physics, Chinese Academy of Sciences.

‡ Department of Chemistry, Tsinghua University.

§ Van't Hoff Institute for Molecular Sciences, Universiteit van Amsterdam.

10.1021/jp0686689 CCC: $37.00
Published on Web 09/21/2007

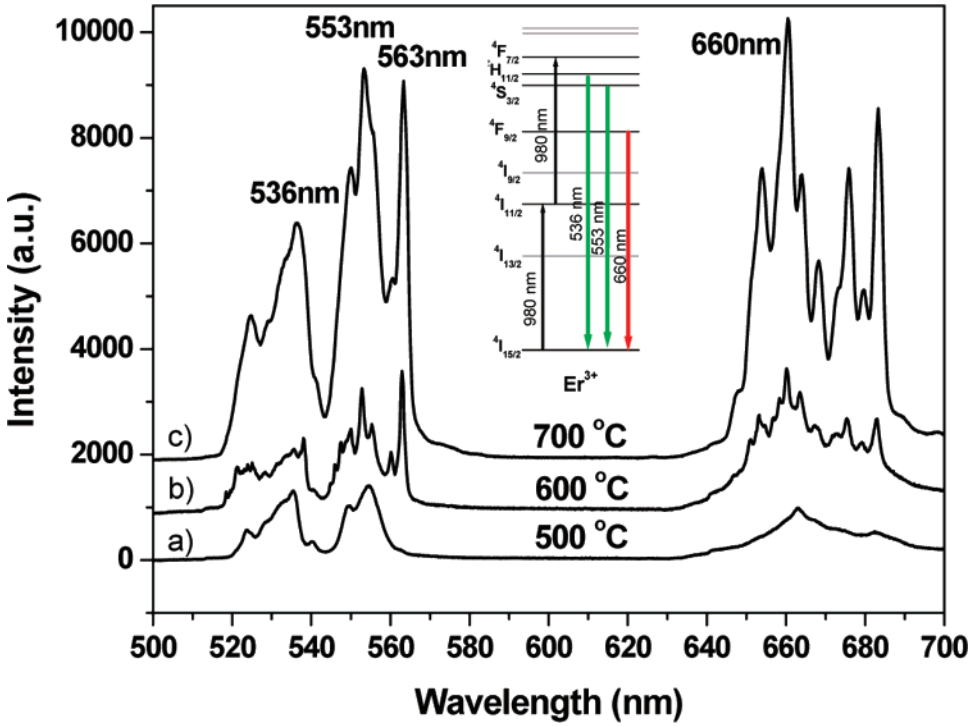

Figure 1. Upconverted luminescence spectra of ZnO:Er^{3+} nanocrystals annealed at (a) 500, (b) 600, and (c) 700 °C. Inset: a simple Er^{3+} ions energy-level diagram for upconversion luminescence processes under 978-nm diode laser exciation.

thermal sensor, as well as semiconductor nanoparticles of CdTe and doped nanoparticles of ZnS:Mn^{2+}, Eu^{3+}.[25] In conjunction with biomolecules (antibodies, nucleic acid, and proteins), nanoscaled ZnO:Er^{3+} could be used as temperature-sensing biosensors, where the upconversion luminescence is particularly interesting because of advantages such as the following: the background emission can be avoided from many biological components (cells and tissues) upon excitation with UV light.

In the present work, we have studied the visible upconversion luminescence properties of Er-doped ZnO nanocrystals with 978-nm light excitation. The green and red upconveted emissions are enhanced distinctly with increasing annealing temperature, which were discussed in terms of multiphonon relaxation assisted by organic group vibrations on the ZnO surface. Of particular interest to us was to utilize the Er^{3+} spectroscopic probe to investigate how the annealing processes influence the local structure of dopant ions in the host material and how the interaction between the dopant ions and the host material influences the spectroscopic properties. Besides, a high thermal sensitivity of 0.0062/°C was obtained based on the temperature-dependent FIR in the ZnO:Er^{3+} nanocrystals.

Experimental Section

The ZnO:Er^{3+} nanocystals were synthesized based on the published procedures with minor modifications.[26,27] A mixture of zinc acetate dihydrate and erbium acetate dihydrate in ethanol was refluxed while stirring for 2−3 h at about 80 °C. After this procedure, a clear Zn−O−Er precursor solution was obtained and then cooled naturally to room temperature (RT). This precursor was hydrolyzed by the addition of lithium hydroxide monohydrate powder with a support of ultrasonic in an ice−water bath for 20 min. A clear ZnO:Er^{3+} colloid solution was obtained after it was filtered through a 0.1-μm glass-fiber filter. The colloid solution was precipitated when adding hexane, and then centrifuged and washed with ethanol. This process was repeated several times. The obtained precipitates were dried at RT in a vacuum oven for 12 h. The dried powder was divided in several parts. One part was kept at RT, and the other parts were annealed at 500, 600, and 700 °C for 30 min, respectively. The annealing processes were performed in air using a heating rate of 10 °C/min. Details on the synthesis of ZnO:Er^{3+} nanocrystals were described elsewhere.[20]

The upconverted luminescence spectra of Er^{3+} ions in the ZnO nanocrystals were recorded on a Jobin-Yvon LabRam Raman spectrometer system equipped with 600 and 1800 grooves/mm holographic grating, and a peltier air-cooled CCD detector. Precise control of sample temperature (±0.1 °C) was achieved by means of a Linkam THMS600 temperature-programmable heating/cooling microscope stage. The THMS stage was used in conjunction with a Linkam LNP cooling system when cooling. Samples were characterized using continuous-wave semiconductor laser diodes centered at 978 nm as an excitation source, matching the $^4I_{15/2} \rightarrow {}^4I_{11/2}$ transition in the 4f energy levels of Er ions perfectly. The FTIR spectra of the samples annealed in different conditions were recorded on the Bio-Rad Excalibur Series FTS 3000MX FTIR spectrometer. The crystalline domain sizes, estimated from the broadening of the X-ray diffraction peaks according to the Scherrer equation, were about 48, 65, and 80 nm for ZnO:Er^{3+} nanocrystals annealed at temperatures of 500, 600, and 700 °C, respectively.[20]

Results and Discussion

A. Annealing Processes Enhancing Upconverted Luminescence. The upconverted luminescence of ZnO:Er^{3+} nanocrystals under 978-nm IR excitation was so strong that can be observed easily with the naked eye. Furthermore, the upconverted luminescence was enhanced with increasing annealing treatment temperature. The RT upconversion emission spectra of ZnO:Er^{3+} nanocrystals, as shown in Figure 1, exhibit three distinct bands in the range of 500−700 nm. The bright-green emissions observed between 500 and 580 nm correspond to the $^2H_{11/2} \rightarrow {}^4I_{15/2}$ and $^4S_{3/2} \rightarrow {}^4I_{15/2}$ transitions; the bright-red

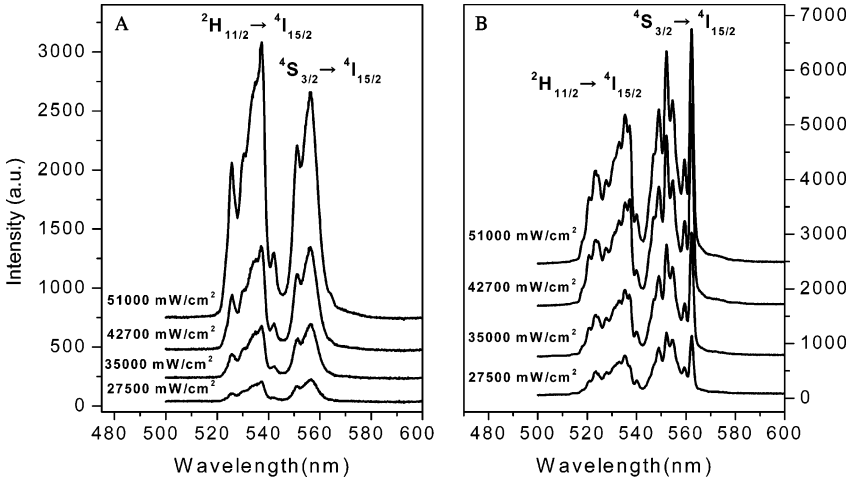

Figure 2. Excitation density dependence of green upconversion spectra of ZnO:Er^{3+} annealed at (A) 500 ($sample_{500}$) and 700 °C ($sample_{700}$), respectively.

emission in the 630−690 nm region is assigned to the $^4F_{9/2} \rightarrow {}^4I_{15/2}$ transition (Inset of Figure 1). To better understand the excitation mechanisms that populate the $^2H_{11/2}$, $^4S_{3/2}$, and $^4F_{9/2}$ levels under near-IR 978-nm light excitation, we studied the pumping-power dependence of the upconversion emission intensity. A logarithmic plot of the integrated emission intensity of the upconverted luminescence as a function of the excitation power, as well as the possible upconversion mechanisms, is shown in Figure S1. The fitting of the data yields a straight line with a slope of approximately 2 for the ($^2H_{11/2}$,$^4S_{3/2}$) $\rightarrow {}^4I_{15/2}$ and $^4F_{9/2} \rightarrow {}^4I_{15/2}$ transitions in all of the samples under investigation, which proves that a two-photon process in the upconversion mechanism is responsible for the green and red emissions. Moreover, Figure 1a−c shows that both green and red upconverted luminescence is distinctly enhanced when the annealing temperature changes from 500 to 700 °C, and the intensity of the sample annealed at 700 °C (defined as $sample_{700}$) is 6 times higher than that of the sample annealed at 500 °C (defined as $sample_{500}$). The observed fine-structured emission bands are related to the rich structure of Er^{3+} multiplet levels in the crystalline ZnO matrix (Figure 1), different from the results of broad bands from the amorphous systems reported by Spanhel.[12] This indicates that the crystal field effect around the Er ions was enhanced, as well as an increase in crystallite size,[28] with increasing annealing temperature.

Note that the observed green and red emissions were enhanced dramatically with increasing annealing temperature. As is well known, an important factor that governs the upconversion efficiency is the nonradiative relaxation rate. Clearly, the presence of C=O and hydroxyl groups with high-frequency stretching modes of about 1500 and 3400 cm^{-1}, respectively, makes multiphonon relaxation fairly efficient (Figure S2). The rate of multiphonon relaxation is dependent upon the energy gap separating the upper and lower states as well as the highest phonon energy in the material.[29] The number of phonons, P, required to complement the energy gap (ΔE) between the upper and lower energy levels can be calculated according to

$$P = \Delta E/\hbar\omega \quad (1)$$

where $\hbar\omega$ is the energy of the phonons in the surrounding medium. The relationship between the nonradiative multiphonon relaxation rate, W_{nr}, and the number of phonons (P) can be determined through the expression

$$W_{nr} = C \exp(-\alpha \cdot P) \quad (2)$$

where both C and α are constants. In addition, the fluorescence quantum yield, η, is related to the radiative and the nonradiative recombination rates, W_r and W_{nr}, expressed by

$$\eta = W_r/(W_r + W_{nr}) \quad (3)$$

Because the presence of the high-frequency vibration modes of 1500 or 3450 cm^{-1} decreases the number of phonons (P) to match the gap of the two energy levels, the nonradiative relaxation rate (W_{nr}) would increase. On the contrary, the fluorescence quantum yield (η) would be depressed. For example, the energy gap of 3680 cm^{-1} between the $^4I_{11/2}$ and $^4I_{13/2}$ levels only requires one or two high-frequency-vibration phonons to bridge. Consequently, the enhancement of upconversion intensities could be rationally attributed to the decrease of the multiphonon relaxation rate due to the decrease of the amount of high-frequency groups (carbonate and hydroxyl) on the ZnO:Er^{3+} surface following an increase of the annealing temperature from 500 to 700 °C. In our previous work,[20] the lifetimes of both the green and red emissions were found to increase for these samples when annealed at higher temperatures, which further indicated the decrease of the nonradiative relaxation. Thus, it could be concluded that the enhancement of the upconverted luminescence of ZnO:Er nanocrystals with high-temperature annealing processes was due to the decrease of the nonradiative relaxation.

B. Annealing Processes Varying Energy Level Configuration of Er Ions. *Excitation-Density Dependence of the Green Upconversion Spectra.* To study the interaction between the dopant ion and the host, we applied the specific properties of Er ions, as sensitive probes, to investigate the variation of the local structure around the Er ions in the ZnO system as well as the structural defects (e.g., point defects) and impurities (e.g., oxygen).[30] The excitation-density dependence of the green upconverted luminescence spectra in $sample_{500}$ and $sample_{700}$ has been measured, as is shown in Figure 2. Here, the area of the illumination spot remains constant on the samples. The overall green upconversion emission in both samples was enhanced when the excitation density increased. For $sample_{500}$, the ratio of the intensity of $^2H_{11/2} \rightarrow {}^4I_{15/2}$ emission to that of $^4S_{3/2} \rightarrow {}^4I_{15/2}$ emission increased from less than to more than unity. For example, at the excitation density of 27 500 W/cm^2, the relative intensity ratio was 0.98 (less than unity), whereas when the excitation density on the sample increases from 35 000 to 51 000 W/cm^2, the emission intensity of the $^2H_{11/2} \rightarrow {}^4I_{15/2}$ transition became more prominent and the ratio went up to 1.08,

TABLE 1: FIR of $^2H_{11/2} \rightarrow {}^4I_{15/2}$ to $^4S_{3/2} \rightarrow {}^4I_{15/2}$ Transitions in ZnO:Er^{3+} Nanocrystals Annealed at 500 and 700 °C, Respectively, Obtained from Upconverted Spectra of Different Excitation Density (ED, Excitation Density; I, Integrated Fluorescent Intensity; FIR, Fluorescence Intensity Ratio of Green Upconverted Emissions)

	sample$_{500}$			sample$_{700}$		
	$^2H_{11/2} \rightarrow {}^4I_{15/2}$	$^4S_{3/2} \rightarrow {}^4I_{15/2}$	FIR	$^2H_{11/2} \rightarrow {}^4I_{15/2}$	$^4S_{3/2} \rightarrow {}^4I_{15/2}$	FIR
ED (W/cm^2)	I_3	I_2	I_3/I_2	I_3	I_2	I_3/I_2
27 500	1664.80	1697.85	0.98	9106.67	13 814.23	0.66
35 000	4789.19	4423.26	1.08	16 806.39	25 327.76	0.66
42 700	9854.35	8510.99	1.16	26 577.90	38 100.63	0.69
51 000	26 409.89	19 289.80	1.37	37 153.93	47 127.88	0.78

1.16, and 1.37 (more than unity). For sample$_{700}$, however, this ratio remained nearly constant (0.66 ± 0.1) until the excitation density went up to 42 700 W/cm^2, from which a slight increase in the ratio was observed (Table 1). An increase of the ratio indicates that the $^2H_{11/2}$ level was populated more efficiently than the $^4S_{3/2}$ level with an increase of the excitation density. For erbium ions, the energy separation between the two nearest excited states $^2H_{11/2}$ and $^4S_{3/2}$ is only several hundred wavenumbers. Once the $^4S_{3/2}$ level was populated, the upper $^2H_{11/2}$ level was populated as well by thermalization owing to Boltzmann distribution. Because of the thermal coupling existing between the $^2H_{11/2}$ and $^4S_{3/2}$ levels, the energy gap between the $^2H_{11/2}$ and $^4S_{3/2}$ levels would contribute significantly to these variations. On the basis of the fact that the thermal population of the $^2H_{11/2}$ level was achieved easily in sample$_{500}$, the energy gap between the $^2H_{11/2}$ and $^4S_{3/2}$ levels could be smaller than that in sample$_{700}$. The energy level of the Er ions in solid hosts experience Stark splitting as the degenerate 4f levels split up in the crystal field caused by the local atomic configuration around the Er^{3+} ions. The energy gap between two close-by levels is determined by the degree of Stark splitting. Accordingly, the crystal field around Er^{3+} in sample$_{700}$ was stronger than that in the sample$_{500}$ because the high-temperature annealing modified the local atomic configuration around the optically active Er^{3+} ions. Both the enhancement of upconversion luminescence and the appearance of a new emission peak at 563 nm provided evidence of a stronger crystal field effect around the Er ions in sample$_{700}$. Further investigation needs to be performed to obtain a better understanding the modification of the chemical environment (such as bond length and O-atom coordination number) around the Er ions by using X-ray absorption fine structure (XRFS) analysis, which has been employed to confirm the symmetry of the local structure of Er degradated to a pseudo-octahedral structure with C_{4v} symmetry in the ZnO:Er film upon annealing at 700 °C.[16] It should be noted that although the microscopic structure around Er was changed drastically during the annealing process, the macroscopic structure of ZnO:Er with a hexagonal phase was fairly stabile.[16,20] Hence, the energy gap between the $^2H_{11/2}$ and the $^4S_{3/2}$ levels was caused mainly by the variation of the crystal field around the Er ion resulting from the modification of its local structure after the annealing at high temperature. Because the thermal effect of near-IR 978-nm light increased the temperature of the sample at the IR light spot, the thermalization population of the $^2H_{11/2}$ level could be further enhanced in sample$_{500}$ because of the smaller energy gap between the $^2H_{11/2}$ and the $^4S_{3/2}$ levels with respect to sample$_{700}$. In addition, thermal conductivity that depends on the size and morphology of the ZnO particles might be another factor in the difference of FIR in the two samples. However, the latter can be neglected considering that it would cause a temperature variation of only several degrees at the excited spot of the samples. Therefore, the growth of the FIR from less than to more than unity with an increase of excitation density for sample$_{500}$ and the independence of the FIR on the excitation density (except when the latter is $>42\ 700$ W/cm^{-2}) for sample$_{700}$ were ascribed mainly to the difference in energy gap between the $^2H_{11/2}$ and $^4S_{3/2}$ states in the two samples.

Measurement-Temperature Dependence of the Green Upconversion Emission. To further identify the distinction and the value of the energy gap between the $^2H_{11/2}$ and $^4S_{3/2}$ levels in the above two samples, we have studied the measurement-temperature dependence of the green upconversion emission spectra under 978-nm excitation, as is shown in Figure 3. The $^2H_{11/2} \rightarrow {}^4I_{15/2}$ emission in both samples was not observed at 77 K. When the measurement temperature increased to 85 K, the emission from the $^2H_{11/2} \rightarrow {}^4I_{15/2}$ transition could be detected for sample$_{500}$, whereas the transition was still not observable for sample$_{700}$ until the measurement temperature was higher than 175 K. When increasing the measurement temperature, an

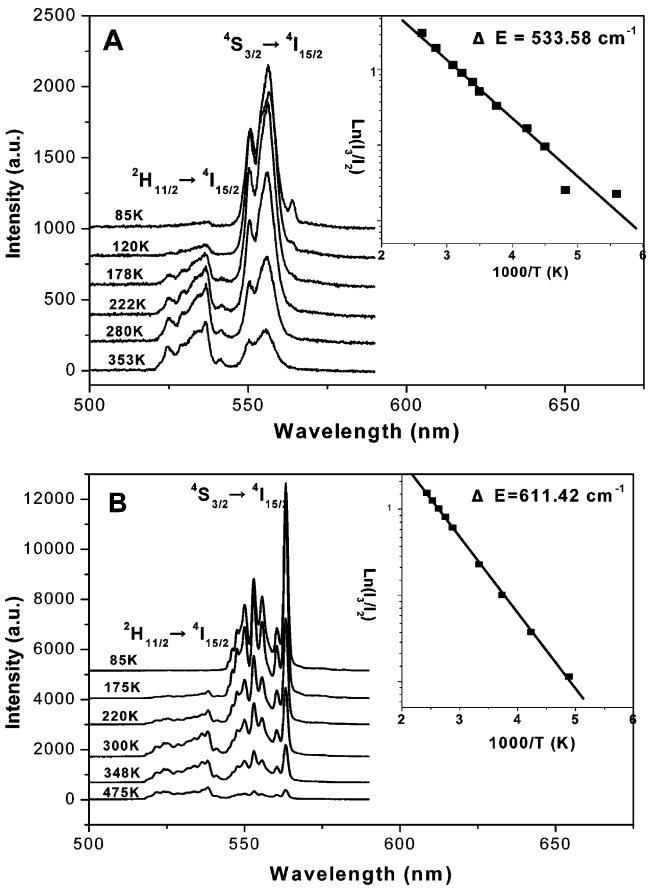

Figure 3. Measurement-temperature dependence of green upconversion spectra in the ZnO:Er^{3+} nanocrystals annealed at (A) 500 and (B) 700 °C, respectively. Inset: logarithm of the integrated intensity ratio of the $^2H_{11/2} \rightarrow {}^4I_{15/2}$ to $^4S_{3/2} \rightarrow {}^4I_{15/2}$ tansitions as a function of inverse absolute temperature ($10^3/T$).

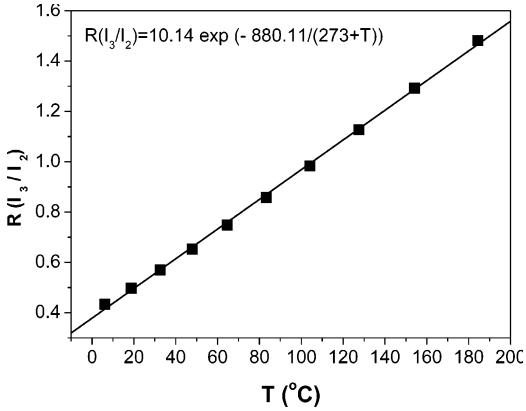

Figure 4. Closely linear relation of green FIR with the temperature (≥0 °C) in the sample annealed at 700 °C.

increase of the fluorescence intensity of the $^2H_{11/2} \rightarrow {}^4I_{15/2}$ transition and a decrease of the $^4S_{3/2} \rightarrow {}^4I_{15/2}$ emission intensity were observed simultaneously. The depopulation of the $^4S_{3/2}$ level, as a feeding level for the $^2H_{11/2}$ level, has contribution to the population of the $^2H_{11/2}$ level because of the thermal distribution between the $^2H_{11/2}$ and $^4S_{3/2}$ levels. The thermalization of the $^2H_{11/2}$ level may be expressed by the following equation[31]

$$\frac{I_3}{I_2} = A \exp\left(-\frac{\Delta E_{32}}{k \cdot T}\right) \tag{4}$$

where I_3 and I_2 are the integrated intensities of the transitions from the $^2H_{11/2}$ and $^4S_{3/2}$ excited states to the $^4I_{15/2}$ ground state, respectively, A is a constant, ΔE_{32} is the energy gap separating the $^2H_{11/2}$ and $^4S_{3/2}$ levels, k is the Boltzmann constant, and T is the absolute temperature. The calculated values of $\ln(I_3/I_2)$ as a function of $1/T$ were fitted to two straight lines, and from their slopes the energy gaps of 534 and 611 cm^{-1} were obtained for $sample_{500}$ and $sample_{700}$, respectively, as shown in the inset of Figure 3. Clearly, the obtained values of the energy gap between the $^2H_{11/2}$ and the $^4S_{3/2}$ levels is smaller in $sample_{500}$ than in $sample_{700}$, in agreement with the fact that the $^2H_{11/2}$ level in $sample_{500}$ is populated more efficiently by thermalization than in $sample_{700}$. The onset temperature at which the $^2H_{11/2} \rightarrow {}^4I_{15/2}$ transition can just be detected in $sample_{500}$ was 85 K, whereas that in $sample_{700}$ was 175 K. This fact further reveals that the relevant thermalization energy is smaller in $sample_{500}$ than in $sample_{700}$. Therefore, it can be concluded that the annealing temperature affects the energy gap between the $^2H_{11/2}$ and the $^4S_{3/2}$ levels of Er^{3+} in the ZnO system.

C. Thermal Sensing and Sensitivity Based on the Green FIR. Temperature-dependent FIR has been employed in thermal sensing, which provides a measure that is essentially independent of the fluctuations in the excitation intensity.[21−23] The thermal sensing effect on the green upconversion fluorescence has also been observed for our samples: the $^2H_{11/2} \rightarrow {}^4I_{15/2}$ and $^4S_{3/2} \rightarrow {}^4I_{15/2}$ emissions varied with the measurement temperature, and the ratio of their fluorescence intensity was the measurement-temperature dependence. Because the FIR in $sample_{700}$ is independent of the variation of the excitation density except above 42 700 W/cm^2, the ratio indeed presents the expected exponential dependence on temperature ($FIR = I_3/I_2 = A \exp(-\Delta E/k_B T)$). From the best fit curve of the data depicted in the inset of Figure 3, $A = 10.14$ and $\Delta E \approx 611$ cm^{-1} are obtained. Figure 4 shows that the value of the FIR, $FIR = 10.14 \exp(-880.11/(273 + T'))$ (T' is in Celsius), is closely linear with sample temperature T' ($T' \geq 0$ °C). For sensing temperature, it

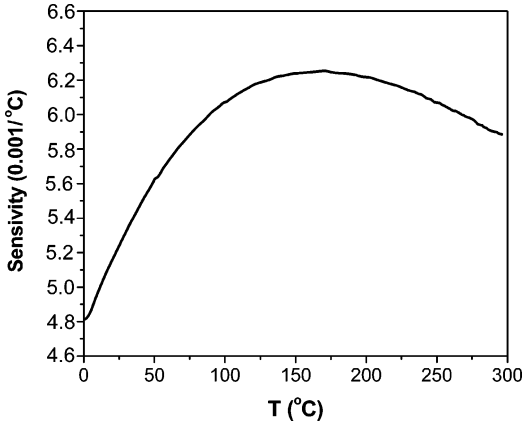

Figure 5. Thermal sensitivity (dR/dT) as a function of temperature obtained from the fitted curve shown in the inset of Figure 4B.

is important to know the rate at which the green FIR varies for a certain change in temperature. This value, known as the thermal sensitivity, S; is given by

$$S = \frac{dR}{dT'} = R\left(\frac{\Delta E}{k_B (T' + 273)^2}\right) \tag{5}$$

The resulting curve of the sensitivity, S; with Celsius degree, T'; is obtained using the Matlab 7.0 software, as shown in Figure 5. The sensitivity reaches maximum of 0.0062/°C at 170 °C in the temperature range of our experiment, which is highly close to the sensitivity (0.0052/°C) reported in the Er/Yb-codoped Ga_2S_3:La_2O_3 chalcogenide glass.[32] This implies that the high thermal sensitivity of 0.0062/°C in the ZnO:Er^{3+} nanocrystals could be potentially applied to design the nanoscale thermal sensor for temperature sensing.

Conclusions

The effect of annealing on the upconversion properties of ZnO:Er^{3+} nanocrystals is significant. The remarkable enhancement of the green and the red upconversion emissions and the increase of the energy gap between the $^2H_{11/2}$ and the $^4S_{3/2}$ levels of Er ions were ascribed to the decrease of the nonradiative relaxation and the enhancement of the crystal field effect around the Er ions, respectively. The excitation-density dependence of the green intensity ratio in $sample_{500}$ implies that the energy gap between the $^2H_{11/2}$ and $^4S_{3/2}$ levels is smaller in $sample_{500}$ than in $sample_{700}$, which is consistent with the obtained energy gap between the $^2H_{11/2}$ and $^4S_{3/2}$ levels in the two samples from the fitted value of the green intensity ratio as a function of temperature. Furthermore, a high thermal sensitivity of 0.0062/°C was obtained from the temperature sensing of green upconverted FIR. On the basis of the temperature-dependent FIR, the ZnO:Er^{3+} nanocrystal is an excellent candidate to be a nanoscale temperature sensor.

Acknowledgment. The work is financially supported by the National Natural Science Foundation of China (60601014, 20603035), "863" (2006AA03Z335), and the Exchange Program between CAS (China)-KNAW (The Netherlands).

Supporting Information Available: Excitation power dependence of the green and red upconverted emission intensities, schematic energy diagram of Er^{3+} with proposed upconversion mechanism under the 978-nm light excitation, and FTIR spectra of the ZnO: Er^{3+} nanocrystals annealed at 500, 600, and 700 °C, respectively, as compared with the as-synthesized ZnO:

Er^{3+} nanocrystals. This material is available free of charge via the Internet at http://pubs.acs.org.

References and Notes

(1) Heer, S.; Kompe, K.; Gudel, H.; Haase, M. *Adv. Mater.* **2004**, *16*, 2102.
(2) Capobianco, J. A.; Vetrone, F.; Boyer, J. C. *J. Phys. Chem. B* **2002**, *106*, 1181.
(3) Vetrone, F.; Boyer, J. C.; Capobianco, J. A.; Speghini, A.; Bettinelli, M. *Chem. Mater.* **2003**, *15*, 2737.
(4) Vetrone, F.; Boyer, J. C.; Capobianco, J. A.; Speghini, A.; Bettinelli, M. *J. Phys. Chem. B* **2002**, *106*, 5622.
(5) Chen, W.; Zhang, J. Z.; Joly, Nanosci, A. J. *Nanotechnol.* **2004**, *4*, 919.
(6) Rijke, F.; Zijlmans, H.; Li, S.; Vail, T.; Raap, A. K.; Niedbala, R. S.; Tanke, H. J. *Nat. Biotechnol.* **2001**, *19*, 273.
(7) Sun, Y.; Liu, H.; Wang, X.; Kong, X.; Zhang, H. *Chem. Mater.* **2006**, *18*, 2726.
(8) Rosa, E.; Salas, P.; Desirena, H.; Angeles, C.; Rodriguez, R. A. *Appl. Phys. Lett.* **2005**, *87*, 241912.
(9) Dosev, D.; Kennedy, I. M.; Godlewski, M.; Gryczynski, I.; Tomsia, K.; Goldys, E. M. *Appl. Phys. Lett.* **2006**, *88*, 011906.
(10) Wang, X.; Shan, G.; Chao, K.; Zhang, Y.; Liu, R.; Feng, L.; Zeng, Q.; Sun, Y.; Liu, Y.; Kong, X. *Mater. Chem. Phys.* **2006**, *99*, 370.
(11) Wang, X.; Shan, G.; An, L.; Chao, K.; Zeng, Q.; Chen, B.; Kong, X. *Acta Phys. Sin.* **2004**, *53*, 1972.
(12) Kohls, M.; Bonanni, M.; Spanhel, L.; Su, D.; Giersig, M. *Appl. Phys. Lett.* **2002**, *81*, 3858.
(13) Kohls, M.; Schmidt, T.; Katschorek, H.; Spanhel, L.; Muller, G.; Mais, N.; Wolf, A.; Forchel, A. *Adv. Mater.* **1999**, *11*, 288.
(14) Komuro, S.; Katsumata, T.; Morikawa, T.; Zhao, X.; Isshiki, H.; Aoyagi, Y. *Appl. Phys. Lett.* **2000**, *76*, 3935.
(15) Komuro, S.; Katsumata, T.; Morikawa, T.; Zhao, X.; Isshiki, H.; Aoyagi, Y. *J. Appl. Phys.* **2000**, *88*, 7129.
(16) Ishii, M.; Komro, S.; Morikawa, T.; Aoyagi, Y. *J. Appl. Phys.* **2001**, *89*, 3679.
(17) Jayakumar, O. D.; Gopalakrishnan, I. K.; Kulshreshtha, S. K. *Adv. Mater.* **2006**, *18*, 1857.
(18) Wang, X.; Kong, X.; Yu, Y.; Zhang, H. *J. Phys. Chem. C* **2007**, *111*, 3836.
(19) Gu, G.; Wang, S.; Lv, M.; Zhou, G.; Xu, D.; Yuan, D. *Langmuir* **2004**, *20*, 3528.
(20) Wang, X.; Kong, X.; Shan, G.; Yu, Y.; Sun, Y.; Feng, L.; Chao, K.; Lu, S.; Li, Y. *J. Phys. Chem. B* **2004**, *108*, 18408.
(21) Sidiroglou, F.; Wade, S. A.; Dragomir, N. M.; Baxter, G. W.; Collins, S. F. *Rev. Sci. Instrum.* **2003**, *74*, 3524.
(22) Wade, S. A.; Collins, S. F.; Baxter, G. W.; Monnom, G. *Rev. Sci. Instrum.* **2001**, *72*, 3180.
(23) Wade, S. A.; Collins, S. F.; Baxter, G. W. *J. Appl. Phys.* **2003**, *94*, 4743.
(24) Collins, S. F.; Baxter, G. W.; Wade, S. A.; Sun, T.; Grattan, T. V.; Zhang, Z. Y.; Palmer, A. W. *J. Appl. Phys.* **1998**, *84*, 4649.
(25) Wang, S.; Westcott, S.; Chen, W. *J. Phys. Chem. B* **2002**, *106*, 11203.
(26) Spanhel, L.; Anderson, M. A. *J. Am. Chem. Soc.* **1991**, *113*, 2826.
(27) Schmidt, T.; Muller, G.; Spanhel. L.; Kerkel, K.; Fouchel, A. *Chem. Mater.* **1998**, *10*, 65.
(28) Noack, V.; Eychmuller, A. *Chem. Mater.* **2002**, *14*, 1411.
(29) Layne, C. B.; Lowdermilk, W. H.; Weber, M. J. *Phys. Rev. B* **1977**, *16*, 10.
(30) Polman, A. *Physica B* **2001**, *300*, 78.
(31) Xu, W.; Dai, S.; Toth, M.; Del Cul, G. D.; Peterson, J. R. *J. Phys. Chem.* **1995**, *99*, 4447.
(32) Samtos, P. V.; Araujo, M. T.; Gouveia Neto, A. S. *Appl. Phys. Lett.* **1998**, *73*, 578.